ACES Asian Chemical Editorial Society

DOI: 10.1002/asia.201701310

CHEMISTRY AN ASIAN JOURNAL Communication

Boron-based Clusters

Dynamic Mg_2B_8 Cluster: A Nanoscale Compass

Ying-Jin Wang[+],[a, b] Lin-Yan Feng[+],[a] Jin-Chang Guo,[a, b] and Hua-Jin Zhai*[a]

Abstract: Boron-based binary cluster Mg_2B_8 is shown to adopt a compass-like structure via computational global searches, featuring an Mg_2 dimer as the needle and a disk-shaped B_8 molecular wheel as baseplate. The nanocompass has a diameter of 0.35 nm. Born–Oppenheimer molecular dynamics simulations indicate that Mg_2B_8 is structurally fluxional with the needle rotating freely on the baseplate, analogous to a functioning compass. The dynamics is readily initiated via a ultrasoft vibrational mode. The rotational barrier is only 0.1 kcal mol^{-1} at the single-point CCSD(T) level. Chemical bonding analysis suggests that the cluster compass can be formulated as $[Mg_2]^{2+}$ $[B_8]^{2-}$; that is, the baseplate and the needle are held together primarily through ionic interactions. The baseplate is doubly aromatic with π and σ sextets. The bonding pattern provides a dilute, continuous, and delocalized electron cloud, which underlies the dynamics of the nanocompass.

Nanomachines are a fantastic dreamland of pursuit in chemistry, materials science, and nanoscience and nanotechnologies.[1,2] Boron-based nanoscale rotors represent a fast expanding topic in the field lately. In particular, a series of molecular Wankel motors (notably B_{19}^- and B_{13}^+)[3–8] and subnanoscale tank treads (B_{11}, B_{11}^-, and B_{15}^+)[9–11] were reported, owing to the electron deficiency of boron, which gives rise to (π and σ) aromaticity, antiaromaticity, and conflicting aromaticity,[12–19] as well as structural fluxionality.[3–11] Boron features a flatland of planar or quasi-planar (2D) clusters up to at least 40 atoms for B_n^-,[19] unlike any other element in the periodic table. Consequently, it seems impractical to uncover or design three-dimensional (3D) fluxional nanosystems solely using boron.

[a] Y.-J. Wang,[+] L.-Y. Feng,[+] Dr. J.-C. Guo, Prof. Dr. H.-J. Zhai
Nanocluster Laboratory
Institute of Molecular Science
Shanxi University
Taiyuan 030006 (P. R. China)
E-mail: hj.zhai@sxu.edu.cn

[b] Y.-J. Wang,[+] Dr. J.-C. Guo
Department of Chemistry
Xinzhou Teachers University
Xinzhou, Shanxi 034000 (P. R. China)

[+] These authors contributed equally to this work.

Supporting information and the ORCID identification number(s) for the author(s) of this article can be found under https://doi.org/10.1002/asia.201701310.

To this end, boron-based doped or mixed clusters come into play. Popov et al. reported two half-sandwich clusters, RhB_{12}^- and CoB_{12}^-, suggesting that complexation with a metal atom can reduce the rotational barrier.[20] Likewise, Liu et al. designed a metal doped molecular Wankel motor, IrB_{12}^-.[21] Li et al. computed a metal-centered tubular rotor, B_2-Ta@B_{18}^-, in which a B_2 dimer rotates almost freely relative to a drum-shaped Ta@B_{18} motif with an energy barrier of 1 kcal mol^{-1}.[22] Very recently, Zhai and co-workers discovered a coaxial triple-layered $Be_6B_{11}^-$ cluster with dual dynamic modes of revolution and rotation, mimicking the earth-moon system at the subnanoscale.[23] Herein we report on the design of a boron-based Mg–B alloy cluster, Mg_2B_8, the unique dynamics of which apes that of a compass. The nanocompass has a diameter of 3.5 Å. The mechanism behind structural fluxionality is elucidated via in-depth bonding analysis.

To locate the global minimum (GM) of Mg_2B_8, we performed global searches using the Coalescence Kick (CK) algorithm.[24,25] Our choice of the present system benefits from two prior computational studies[26,27] on relevant binary clusters, although dynamic fluxionality is either not recognized or not possible in those systems.[28] For the Mg_2B_8 cluster in this work, a total of 3000 stationary points were probed on the potential energy surface in the CK global searches. Low-lying isomers were subsequently reoptimized at the PBE0/6-311+G* level. Top isomers are presented in the Supporting Information (Figure S1), and the top three isomers were further benchmarked at single-point CCSD(T)/6-311+G*//PBE0/6-311+G* level[29,30] for accurate energetics. The PBE0 and CCSD(T) data are highly consistent, firmly establishing the C_s ($^1A'$) structure as the GM of Mg_2B_8 cluster, as illustrated in Figure 1a. The GM has a nearly planar B_8 wheel with an Mg_2 unit sitting on the top. The closest competitor, D_{8h} ($^1A_{1g}$), has an eight-membered B ring, with the Mg–Mg axis being perpendicularly oriented. It is 0.23 eV higher in energy at single-point CCSD(T), suggesting that the GM is reasonably well-defined. The energetics of C_s versus D_{8h} isomers in Mg_2B_8 and its isovalent Be_2B_8 species[27] is an interesting issue, which leads to the favorable C_s structure for Mg_2B_8 but not for Be_2B_8 (Figure 2),[31] the latter cluster being thus nonfluxional.

The GM of Mg_2B_8 cluster has uniform peripheral and radial B–B bond distances of 1.55–1.56 and 1.78–1.80 Å, respectively (Figure S2a), at PBE0 level, indicative of a circular B_8 wheel. Out-of-plane distortion of the wheel amounts to 0.17 Å only. The former B–B distances are markedly shorter than single bond (upper limit: 1.70 Å),[32] whereas the latter ones are longer than single bond. Nonetheless, all these distances are virtually identical to those in bare D_{7h} B_8^{2-} molecular wheel

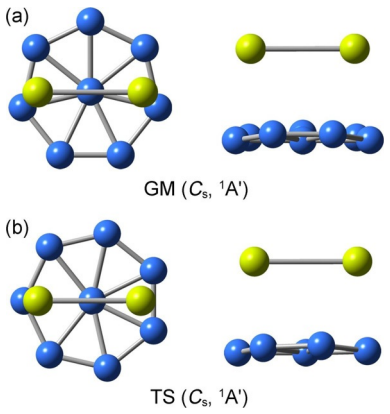

Figure 1. Optimized structures of a) C_s (^{1}A′) global minimum (GM) and b) C_s (^{1}A′) transition state (TS) of the Mg_2B_8 cluster at PBE0/6-311+G* level. Both top- and side-views are presented.

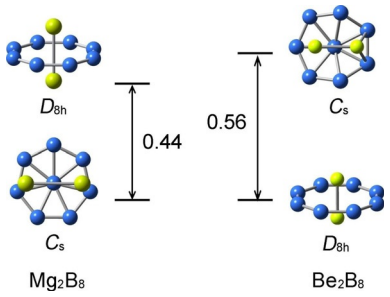

Figure 2. Comparison of the energetics of two typical isomeric structures of Mg_2B_8 and Be_2B_8. The two isovalent clusters have distinct global-minimum (GM) structures. Relative energies are shown in eV at PBE0/6-311+G* level, with corrections for zero-point energies (ZPEs).

(1.55 versus 1.79 Å),[12] hinting that the B_8 wheel in Mg_2B_8 cluster is probably relevant to the gas-phase B_8^{2-} cluster. The Mg–Mg distance is 2.68 Å, shorter than those of Mg–Mg covalent bonds containing Mg in oxidation state "+1" in LMg–MgL compounds (2.82–2.94 Å),[33–36] which suggests that the Mg_2 unit in Mg_2B_8 should carry a substantial amount of positive charges (*vide infra*). Note that the recommended distance of Mg–Mg single bond is 2.78 Å.[32] On the other hand, the Mg–B distance between the Mg_2 dimer and B_8 wheel is as large as 2.42 Å, hinting relatively weak Mg–B bonding (single bond: 2.24 Å).

Wiberg bond indices (WBIs) from natural bond orbital (NBO) analysis support the above assignments (Figure S3 a). WBIs for peripheral B–B bonds are 1.34–1.37, indicating delocalized bonding beyond a two-center two-electron (2c–2e) σ bond. Similarly, radial B–B bonds have WBIs of 0.50–0.56, suggesting delocalized bonding within the B_8 wheel. The Mg–Mg bond has a WBI of 0.85, which is close to a single bond and comparable to that in Mg_2Cl_2 (WBI: 0.94). Not surprisingly, NBO analysis reveals that the Mg atoms each carry a positive charge of 0.70 |e| (Figure S4), confirming that the Mg_2B_8 nanocompass is best described as $[Mg_2]^{2+}[B_8]^{2-}$. In line with the formula, the WBIs for Mg–B links are negligibly small (0.11–0.13), which are far weaker than other bonds in the cluster, offering possibility for a dynamic and fluxional system.

Vibrational frequency analysis indicates that the GM of Mg_2B_8 has a soft mode of 10.3 cm^{-1} at PBE0 level (Figure S5). This mode corresponds to the rotation of Mg_2 dimer on the B_8 wheel, in which seven peripheral B atoms move in phase tangentially, countering the direction of two Mg atoms. Following the mode, a transition state (TS) is located; see Figure 1 b. The TS structure also has C_s symmetry, with a soft imaginary mode of 5.1*i* cm^{-1}. These soft modes for rotation are independently checked and confirmed at the TPSSH level as well, which should facilitate nearly free rotation of Mg_2 on the B_8 wheel. Born-Oppenheimer molecular dynamics (BOMD) simulations vividly confirm this idea. The simulations were done at temperatures of 200, 400, and 600 K, at the PBE/DZVP level,[37] starting from the equilibrium GM geometry with random velocities assigned to the atoms. During the simulations, the Mg_2 and B_8 fragments in Mg_2B_8 always maintain their identities (that is, structural integrity), and yet they do rotate with respect to each other as anticipated, even at 200 K (well below room temperature), akin to a functioning compass. An extracted short movie from a simulation of over 50 ps at 600 K is presented as an example in the Supporting Information. The movie covers a time span of roughly 10 ps.

Quantitatively, the rotational barrier is almost zero at the PBE0 level. It is refined to 0.1 kcal mol^{-1} at single-point CCSD(T). Figure 3 illustrates the structural evolution of the Mg_2B_8 nanocompass in action, assuming that the Mg_2 needle rotates clockwise. At starting structure GM_1, the Mg9Mg10 needle floats on B_8 baseplate, with the central B8 atom serving as fulcrum and the Mg9–B6 and Mg10–B3 links being the shortest. As Mg9 moves clockwise following the soft mode (by 12.8°), the Mg9–Mg10 axis becomes perpendicular to the B6–B7 link in baseplate and aligned perfectly with the radial B8–B3 link, generating the first TS structure (TS_{1-2}). Going down the barrier, GM_2 is reached with the Mg9Mg10 needle rotating by another 12.8°. GM_2 can be viewed as a reflection of GM_1 via the B8–B3 axis. The evolution from GM_2 to GM_3 is closely in the spirit of that from GM_1 to GM_2. GM_3 is a reflection of GM_2 via the B8–B7 axis, whereas in TS_{2-3} the Mg9Mg10 needle aligns with the radial B8–B7 link. Overall, from GM_1 to GM_3, the Mg9Mg10 needle rotates by one peripheral B–B link (or 51.4°).

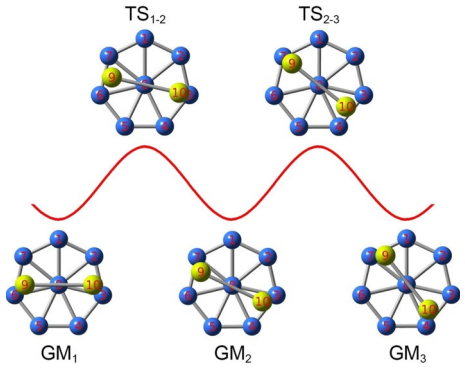

Figure 3. Structural evolution of Mg_2B_8 cluster during the dynamic rotation of Mg_2 dimer with respect to the B_8 baseplate. The Mg_2 dimer is assumed to rotate clockwise in the presentation.

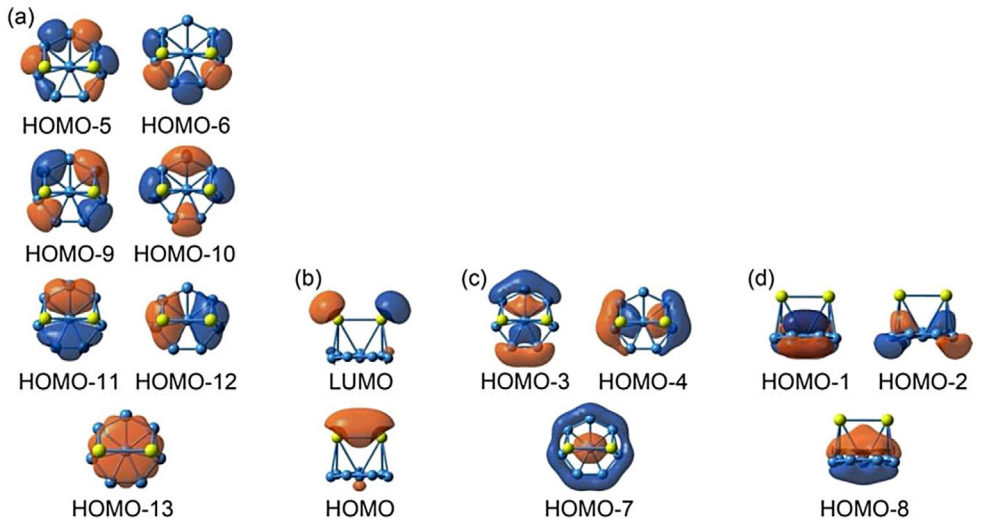

Figure 4. Canonical molecular orbitals (CMOs) of the C_s ($^1A'$) GM structure of Mg_2B_8 cluster. a) Seven CMOs for localized B–B σ bonds in the periphery of B_8 wheel. b) One σ bond within the Mg_2 unit, as well as the LUMO. c) Three delocalized σ CMOs. d) Three delocalized π CMOs. Subsets in c) and d) render the Mg_2B_8 cluster (π and σ) double aromaticity.

Repeating the above process for 7 times and every atom in the cluster restores its exact initial position.

To rationalize the dynamics of Mg_2B_8 as a nanoscale compass, it is essential to perform chemical bonding analysis. Canonical molecular orbitals (CMOs) of the GM are depicted in Figure 4, which are sorted into four subsets. Of the 14 CMOs (28 valence electrons) in the system, only HOMO is Mg 3s based (Figure 4b), defining an Mg–Mg σ bond for the Mg_2 needle. Its corresponding antibonding CMO (that is, the LUMO) is empty due to intramolecular charge transfers of 2 electrons from Mg_2 to B_8, resulting in an $[Mg_2]^{2+}[B_8]^{2-}$ complex as stated earlier, which compensates for the electron-deficiency of boron and in the meantime strengthens Mg-Mg interaction. Intuitively, the Mg_2–B_8 ionic interaction in the system is anticipated to be quite strong, because there exist two ionic bonds formally. Thus, dynamic fluxionality of Mg_2B_8 nanocompass is not due to "weak" Mg_2–B_8 interaction. Nevertheless, it is a complicated technical issue to quantify the strength of this interaction. As an estimate, we manually separate the Mg_2 and B_8 fragments to a large distance of 10 Å (at which ionic interaction decreases substantially) and do a single-point PBE0/6-311+G* calculation. The energy difference (4.79 eV), with respect to the GM structure, is largely attributable to Mg_2–B_8 ionic interaction. We stress that the above estimate is qualitative rather than quantitative.

All other CMOs of Mg_2B_8 are attributable to the $[B_8]^{2-}$ wheel. Shown in Figure 4a are seven σ CMOs that are primarily composed of B 2s based atomic orbitals (AOs) from the peripheral ring, with from 0 up to 3 nodal planes along the series. This subset represents seven localized 2c–2e σ bonds. The three CMOs in Figure 4d form a π sextet akin to that in benzene, rendering π aromaticity to Mg_2B_8. Likewise, three delocalized σ CMOs (Figure 4c) show one-to-one correspondence to those of π sextet. This σ sextet cannot be transformed to Lewis elements, making it imperative to claim σ aromaticity. Thus, the Mg_2B_8 cluster is doubly aromatic owing to its π and σ sextets.

The bonding picture is faithfully borne out from adaptive natural density partitioning (AdNDP),[38] an extension of the NBO analysis. As shown in Figure 5, AdNDP clearly recovers one 2c–2e Mg–Mg σ bond for the Mg_2 needle, as well as seven peripheral 2c–2e B–B σ bonds and delocalized π and σ sextets for the B_8 baseplate. The π and σ double aromaticity provides delocalized, continuous electron cloud in the nanocompass, which underlies its dynamics. In such a unique bonding situation, any individual Mg–B bond or radial B–B bond does not exist. Instead, the B_8 baseplate serves as a uniform, circular disk of π and σ cloud, on which the Mg_2 needle slides freely. Nucleus-independent chemical shifts, NICS and $NICS_{ZZ}$, are calculated for Mg_2B_8 as an additional criterion for aromaticity (Table S1). The large negative values are consistent with the assessment of π and σ double aromaticity. Furthermore, the HOMO–LUMO gap is calculated to be 3.38 eV at PBE0/6-311+

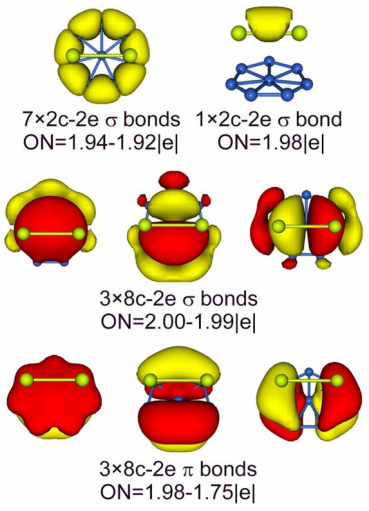

Figure 5. AdNDP bonding pattern for the C_s ($^1A'$) GM of Mg_2B_8 cluster. Occupation numbers (ONs) are shown.

G*, demonstrating the electronic robustness of Mg_2B_8 nanocompass. The CMO and AdNDP patterns of the TS structure are similar to those of the GM, except for a spatial shift of electron cloud (Figures S6 and S7). Indeed, the geometries of Mg_2 needle and B_8 baseplate virtually do not change from GM to TS (within 0.01 Å), neither do the NBO charges (within 0.04 | e |) and WBIs (within 0.02). In particular, the WBIs for Mg–B links are 0.11–0.13 for GM versus 0.12–0.13 for TS, which are extremely weak and remain constant during dynamic motions. This explains why the rotational barrier is negligible, because it is the variation of WBIs between GM and TS that governs the barrier height.

Interestingly, BOMD simulations show that the Mg_2 needle floats on B_8 baseplate, and yet there seems to be an anchor point for the needle. The "mysterious" anchor point is in the middle of Mg_2, which connects the needle to the central B atom in baseplate. The connection is executed partly by HOMO and HOMO–8 (Figure 4), in which the downward and upward tips in electron cloud, respectively, help configure and optimize the geometry of Mg_2B_8 cluster, ensuring that the Mg_2 needle does not slip away from the baseplate during dynamic motions. Indeed, orbital component analysis indicates that HOMO–8 contains 20% of Mg 3s contribution.

In conclusion, we have demonstrated that boron-based binary cluster, Mg_2B_8, is structurally fluxional and behaves like a nanocompass, which consists of a wheel-like B_8 baseplate and an Mg_2 needle. It gains stability due to intramolecular charge transfers that lead to the $[Mg_2]^{2+}[B_8]^{2-}$ formula, as well as π and σ sextets for double aromaticity in B_8 baseplate. The bonding pattern helps lubricate the structural dynamics of the nanocompass, with a near zero energy barrier for rotation. The Mg_2B_8 nanocompass is intriguing, as is its bonding mechanism. We anticipate other nanocompass clusters and fluxional nanosystems to be designed and fabricated in the forthcoming years.

Methods Section

Global-minimum searches were carried out using the unbiased CK method[24,25] at the density-functional theory (DFT) level. Low-lying isomers were then fully reoptimized and their relative energies evaluated at PBE0/6–311+G*, using the Gaussian 09 package.[39] Vibrational frequencies were calculated at the same level to ensure that the reported structures are true minima. To obtain accurate energetics for top isomers and the TS structure, further calculations were done at single-point CCSD(T)/6–311+G*//PBE0/6–311+G* level.[29,30] Chemical bonding was elucidated via CMO analysis and AdNDP,[38] the latter being done at PBE0/6-31G. NBO bond indices were obtained at PBE0/6–311G* level. NICS data were calculated at PBE0/6–311+G*. BOMD simulations were accomplished using the CP2K software package.[37] The visualization of AdNDP results was realized using the Molekel 5.4.0.8 program.[40]

Acknowledgements

This work was supported by the National Natural Science Foundation of China (21573138) and the Sanjin Scholar Distinguished Professors Program. Additional support was provided by the Natural Science Fund of Xinzhou Teachers University (201711), the Scientific and Technological Innovation Programs of Higher Education Institutions in Shanxi (2017170), and the China Postdoctoral Science Foundation (2017M611193).

Conflict of interest

The authors declare no conflict of interest.

Keywords: boron-based clusters · chemical bonding · molecular dynamics · nanoscale compass · structural fluxionality

[1] C. Joachim, G. Rapenne, *ACS Nano* **2013**, *7*, 11.
[2] Y. Shirai, J. F. Morin, T. Sasaki, J. M. Guerrero, J. M. Tour, *Chem. Soc. Rev.* **2006**, *35*, 1043.
[3] J. O. C. Jiménez-Halla, R. Islas, T. Heine, G. Merino, *Angew. Chem. Int. Ed.* **2010**, *49*, 5668; *Angew. Chem.* **2010**, *122*, 5803.
[4] G. Martínez-Guajardo, A. P. Sergeeva, A. I. Boldyrev, T. Heine, J. M. Ugalde, G. Merino, *Chem. Commun.* **2011**, *47*, 6242.
[5] D. Moreno, S. Pan, L. L. Zeonjuk, R. Islas, E. Osorio, G. Martínez-Guajardo, P. K. Chattaraj, T. Heine, G. Merino, *Chem. Commun.* **2014**, *50*, 8140.
[6] S. Jalife, L. Liu, S. Pan, J. L. Cabellos, E. Osorio, C. Lu, T. Heine, K. J. Donald, G. Merino, *Nanoscale* **2016**, *8*, 17639.
[7] T. B. Tai, A. Ceulemans, M. T. Nguyen, *Chem. Eur. J.* **2012**, *18*, 4510.
[8] M. R. Fagiani, X. Song, P. Petkov, S. Debnath, S. Gewinner, W. Schöllkopf, T. Heine, A. Fielicke, K. R. Asmis, *Angew. Chem. Int. Ed.* **2017**, *56*, 501; *Angew. Chem.* **2017**, *129*, 515.
[9] Y. J. Wang, X. Y. Zhao, Q. Chen, H. J. Zhai, S. D. Li, *Nanoscale* **2015**, *7*, 16054.
[10] Y. J. Wang, X. R. You, Q. Chen, L. Y. Feng, K. Wang, T. Ou, X. Y. Zhao, H. J. Zhai, S. D. Li, *Phys. Chem. Chem. Phys.* **2016**, *18*, 15774.
[11] Y. J. Wang, J. C. Guo, H. J. Zhai, *Nanoscale* **2017**, *9*, 9310.
[12] H. J. Zhai, A. N. Alexandrova, K. A. Birch, A. I. Boldyrev, L. S. Wang, *Angew. Chem. Int. Ed.* **2003**, *42*, 6004; *Angew. Chem.* **2003**, *115*, 6186.
[13] H. J. Zhai, B. Kiran, J. Li, L. S. Wang, *Nat. Mater.* **2003**, *2*, 827.
[14] A. N. Alexandrova, A. I. Boldyrev, H. J. Zhai, L. S. Wang, *Coord. Chem. Rev.* **2006**, *250*, 2811.
[15] W. Huang, A. P. Sergeeva, H. J. Zhai, B. B. Averkiev, L. S. Wang, A. I. Boldyrev, *Nat. Chem.* **2010**, *2*, 202.
[16] W. L. Li, Q. Chen, W. J. Tian, H. Bai, Y. F. Zhao, H. S. Hu, J. Li, H. J. Zhai, S. D. Li, L. S. Wang, *J. Am. Chem. Soc.* **2014**, *136*, 12257.
[17] B. Kiran, S. Bulusu, H. J. Zhai, S. Yoo, X. C. Zeng, L. S. Wang, *Proc. Natl. Acad. Sci. USA* **2005**, *102*, 961.
[18] A. P. Sergeeva, D. Y. Zubarev, H. J. Zhai, A. I. Boldyrev, L. S. Wang, *J. Am. Chem. Soc.* **2008**, *130*, 7244.
[19] H. J. Zhai, Y. F. Zhao, W. L. Li, Q. Chen, H. Bai, H. S. Hu, Z. A. Piazza, W. J. Tian, H. G. Lu, Y. B. Wu, Y. W. Mu, G. F. Wei, Z. P. Liu, J. Li, S. D. Li, L. S. Wang, *Nat. Chem.* **2014**, *6*, 727.
[20] I. A. Popov, W. L. Li, Z. A. Piazza, A. I. Boldyrev, L. S. Wang, *J. Phys. Chem. A* **2014**, *118*, 8098.
[21] L. Liu, D. Moreno, E. Osorio, A. C. Castro, S. Pan, P. K. Chattaraj, T. Heine, G. Merino, *RSC Adv.* **2016**, *6*, 27177.
[22] W. L. Li, T. Jian, X. Chen, H. R. Li, T. T. Chen, X. M. Luo, S. D. Li, J. Li, L. S. Wang, *Chem. Commun.* **2017**, *53*, 1587.
[23] J. C. Guo, L. Y. Feng, Y. J. Wang, S. Jalife, A. Vásquez-Espinal, J. L. Cabellos, S. Pan, G. Merino, H. J. Zhai, *Angew. Chem. Int. Ed.* **2017**, *56*, 10174; *Angew. Chem.* **2017**, *129*, 10308.
[24] M. Saunders, *J. Comput. Chem.* **2004**, *25*, 621.
[25] P. P. Bera, K. W. Sattelmeyer, M. Saunders, H. F. Schaefer, P. v. R. Schleyer, *J. Phys. Chem. A* **2006**, *110*, 4287.
[26] A. C. Reber, S. N. Khanna, *J. Chem. Phys.* **2015**, *142*, 054304.
[27] Z. H. Cui, W. S. Yang, L. Zhao, Y. H. Ding, G. Frenking, *Angew. Chem. Int. Ed.* **2016**, *55*, 7841; *Angew. Chem.* **2016**, *128*, 7972.
[28] Reber and Khanna[26] explored geometries and electronic structure of $Mg_mB_n^-$ ($m=0$–3; $n=1$–15) clusters, albeit without global searches. Cui et al.[27] reported unusually short Be–Be distances in Be_2B_8 and $Be_2B_7^-$

despite the nonexistence of Be–Be bonding therein. However, no dynamic properties are unveiled or speculated in the former study; whereas Be_2B_8 and $Be_2B_7^-$ species in the latter do not assume compass-like geometries and are thus not dynamically fluxional.

[29] R. Krishnan, J. S. Binkley, R. Seeger, J. A. Pople, *J. Chem. Phys.* **1980**, *72*, 650.

[30] C. Adamo, V. Barone, *J. Chem. Phys.* **1999**, *110*, 6158.

[31] Generally speaking, the C_s structure has a wheel-like B_8^{2-} moiety and benefits from one M–M bond (M = Mg, Be), as well as the strengthened π and σ sextets due to the central B atom. In contrast, the D_{8h} structure features a formal B_8^{4-} monocyclic ring, which has one extra peripheral B–B bond, no M–M bond, and weaker π and σ sextets. For Mg_2B_8, the C_s structure has a clear advantage (Figure 2). For Be_2B_8, the D_{8h} structure allows Be atoms to participate effectively in both π and σ sextets due to the Be–B covalency in bonding; whereas its C_s structure is highly distorted from planarity, resulting in poor π and σ delocalization. Consequently, nanocompass structure is not favorable for the Be_2B_8 system.[27] For the exact amount of intramolecular charge transfers, those for C_s and D_{8h} structures of Mg_2B_8 are 1.40 and 2.80 |e|, respectively, compared to 1.04 and 1.70 |e| for Be_2B_8.

[32] P. Pyykkö, *J. Phys. Chem. A* **2015**, *119*, 2326.

[33] S. P. Green, C. Jones, A. Stasch, *Science* **2007**, *318*, 1754.

[34] Y. Liu, S. Li, X. Yang, P. Yang, B. Wu, *J. Am. Chem. Soc.* **2009**, *131*, 4210.

[35] S. J. Bonyhady, D. Collis, G. Frenking, N. Holzmann, C. Jones, A. Stasch, *Nat. Chem.* **2010**, *2*, 865.

[36] A. J. Boutland, D. Dange, A. Stasch, L. Maron, C. Jones, *Angew. Chem. Int. Ed.* **2016**, *55*, 9239; *Angew. Chem.* **2016**, *128*, 9385.

[37] J. VandeVondele, M. Krack, F. Mohamed, M. Parrinello, T. Chassaing, J. Hutter, *Comput. Phys. Commun.* **2005**, *167*, 103.

[38] D. Y. Zubarev, A. I. Boldyrev, *Phys. Chem. Chem. Phys.* **2008**, *10*, 5207.

[39] M. J. Frisch, G. W. Trucks, H. B. Schlegel, G. E. Scuseria, M. A. Robb, J. R. Cheeseman, G. Scalmani, V. Barone, B. Mennucci, G. A. Petersson, H. Nakatsuji, M. Caricato, X. Li, H. P. Hratchian, A. F. Izmaylov, J. Bloino, G. Zheng, J. L. Sonnenberg, M. Hada, M. Ehara, K. Toyota, R. Fukuda, J. Hasegawa, M. Ishida, T. Nakajima, Y. Honda, O. Kitao, H. Nakai, T. Vreven, J. A. Montgomery, Jr., J. E. Peralta, F. Ogliaro, M. Bearpark, J. J. Heyd, E. Brothers, K. N. Kudin, V. N. Staroverov, R. Kobayashi, J. Normand, K. Raghavachari, A. Rendell, J. C. Burant, S. S. Iyengar, J. Tomasi, M. Cossi, N. Rega, J. M. Millam, M. Klene, J. E. Knox, J. B. Cross, V. Bakken, C. Adamo, J. Jaramillo, R. Gomperts, R. E. Stratmann, O. Yazyev, A. J. Austin, R. Cammi, C. Pomelli, J. W. Ochterski, R. L. Martin, K. Morokuma, V. G. Zakrzewski, G. A. Voth, P. Salvador, J. J. Dannenberg, S. Dapprich, A. D. Daniels, Ö. Farkas, J. B. Foresman, J. V. Ortiz, J. Cioslowski, D. J. Fox, Gaussian 09, Revision D.01, Gaussian, Inc., Wallingford CT, **2009**.

[40] U. Varetto, Molekel 5.4.0.8, Swiss National Supercomputing Center, Manno (Switzerland), **2009**.

Manuscript received: September 8, 2017
Revised manuscript received: September 26, 2017
Accepted manuscript online: September 26, 2017
Version of record online: October 20, 2017